

A unifying principle underlying the extracellular field potential spectral responses in the human cortex

Ella Podvalny,^{1,2} Niv Noy,^{1,2} Michal Harel,¹ Stephan Bickel,^{3,4} Gal Chechik,² Charles E. Schroeder,^{5,6} Ashesh D. Mehta,⁴ Misha Tsodyks,¹ and Rafael Malach¹

¹Department of Neurobiology, Weizmann Institute of Science, Rehovot, Israel; ²Gonda Multidisciplinary Brain Research Center, Bar Ilan University, Ramat Gan, Israel; ³Department of Neuroscience, Albert Einstein College of Medicine, Bronx, New York; ⁴Department of Neurosurgery, Hofstra North Shore LIJ School of Medicine and Feinstein Institute for Medical Research, Manhasset, New York; ⁵Cognitive Neuroscience and Schizophrenia Program, Nathan Kline Institute, Orangeburg, New York; and ⁶Department of Psychiatry, Columbia College of Physicians and Surgeons, New York, New York

Submitted 24 November 2014; accepted in final form 6 April 2015

Podvalny E, Noy N, Harel M, Bickel S, Chechik G, Schroeder CE, Mehta AD, Tsodyks M, Malach R. A unifying principle underlying the extracellular field potential spectral responses in the human cortex. *J Neurophysiol* 114: 505–519, 2015. First published April 8, 2015; doi:10.1152/jn.00943.2014.—Electrophysiological mass potentials show complex spectral changes upon neuronal activation. However, it is unknown to what extent these complex band-limited changes are interrelated or, alternatively, reflect separate neuronal processes. To address this question, intracranial electrocorticograms (ECoG) responses were recorded in patients engaged in visuomotor tasks. We found that in the 10- to 100-Hz frequency range there was a significant reduction in the exponent χ of the $1/f^\chi$ component of the spectrum associated with neuronal activation. In a minority of electrodes showing particularly high activations the exponent reduction was associated with specific band-limited power modulations: emergence of a high gamma (80–100 Hz) and a decrease in the alpha (9–12 Hz) peaks. Importantly, the peaks' height was correlated with the $1/f^\chi$ exponent on activation. Control simulation ruled out the possibility that the change in $1/f^\chi$ exponent was a consequence of the analysis procedure. These results reveal a new global, cross-frequency (10–100 Hz) neuronal process reflected in a significant reduction of the power spectrum slope of the ECoG signal. ECoG; electrophysiology; power spectrum; $1/f$; narrow-band gamma

A MAJOR ADVANCE in our understanding of human cortical function has been obtained through invasive recordings, conducted for clinical purposes in epilepsy patients (e.g., Mukamel and Fried 2011). The more common method applied in such diagnostic procedure has been electrocorticogram (ECoG) recordings, which are mass potentials, obtained from small electrodes placed directly on the cortical surface. In parallel with extensive research in nonhuman primates, it has been established that the frequency content of such electrophysiological signals is modulated by mental states and behavior (Buzsáki and Draguhn 2004; Fries et al. 2001; Gray and Singer 1989; Henrie and Shapley 2005). A large body of research has been focused on attempts to characterize the functional roles that specific frequency bands play in cortical processing (Buzsaki 2006).

Previous ECoG studies revealed a stimulus-related broadband power increase in the frequency range of 40–150 Hz during visual, motor, and auditory tasks (Crone et al. 2001;

Fisch et al. 2009; Lachaux et al. 2000; Miller et al. 2009; Nir et al. 2007; Ossandón et al. 2012; Privman et al. 2007). At the low frequencies, power decreases (also termed event-related desynchronization, ERD) were reported during sensory activation (Berger 1929; Chatrian 1976; Pfurtscheller and Aranibar 1977; Ramot et al. 2012). A clear association between the broadband gamma increase and neuronal firing on the one hand (Manning et al. 2009; Mukamel et al. 2005; Nir et al. 2007) and the ERD on the other has been reported (Crone et al. 1998b; Mukamel et al. 2005; Ramot et al. 2012).

In parallel, numerous studies have demonstrated that the LFP and ECoG signals span a broad range of frequencies that follow a $1/f^\chi$ function, where the power is inversely proportional to frequency, f , with a scaling exponent χ (Dehghani et al. 2010; Freeman and Zhai 2009; He et al. 2010; Henrie and Shapley 2005; Manning et al. 2009; Miller et al. 2009; Milstein et al. 2009; Nir et al. 2008; Pritchard 1992). Although this power to frequency “power law” relation is ubiquitous in neuronal activity, its function and origin are still unclear (Bak et al. 1987; Bédard and Destexhe 2009; He 2014). The $1/f^\chi$ component was often considered either as noise or attributed to the frequency-dependent filtering properties of the extracellular medium (Bédard et al. 2004). More recently, the frequency-dependent filtering hypothesis was ruled out (Logothetis et al. 2007) and the $1/f^\chi$ spectrum was suggested to be related to neural activity (El Boustani et al. 2009; He et al. 2010; Nir et al. 2008). While these findings begin to reveal the full extent of spectral responses in neural populations, the relation between different spectral components remains unclear.

Consequently, our aim in this study was to search for possible relationship between the different ECoG spectral characteristics: the broadband $1/f^\chi$ component and the band-limited “bumps” appearing on top of the broadband component. To that end, we separated these components of the spectrum and analyzed them independently. Our results reveal a global reduction in the exponent of the $1/f^\chi$ component spanning a wide frequency range (10–100 Hz). In a minority of electrodes showing particularly high responsivity, we found also modulations in band-limited peaks appearing on top of the $1/f^\chi$ component in the alpha and gamma range. The peaks' height was correlated to the exponent χ , thus suggesting a link between broadband and band-limited spectral phenomena.

Address for reprint requests and other correspondence: R. Malach, Dept. of Neurobiology, Weizmann Institute of Science, Rehovot 76100, Israel (e-mail: rafi.malach@gmail.com).

MATERIALS AND METHODS

Subjects and Data Collection

Six subjects participated in the present study [4 women, 27.5 ± 3.9 yr old (mean \pm SE), see Table 1 for details] with pharmacologically intractable epilepsy, monitored for presurgical evaluation. The recordings were conducted at the patients' quiet bedside. Stimuli were presented via a standard LCD screen and keyboard responses were recorded. The data were collected in Long Island Jewish Medical Center, New York, and Columbia University Medical Center, New York. All patients provided fully informed written consent according to the US National Institutes of Health guidelines, as monitored by the local institutional review boards, which approved the study protocol. Each patient was implanted with 104–126 intracranial electrodes for 5–10 days. The electrodes were arranged in subdural grids, strips, and/or depth arrays (Integra Lifesciences). In the subdural grids and strips, each recording site was 2 mm in diameter with 1 cm separation, whereas in the depth electrodes each recording site was 1 mm in diameter with 0.5 cm separation. The location and number of electrodes were based solely on clinical criteria. The signals were filtered electronically between 0.5–500 Hz or 0.1 Hz–1 kHz and sampled at a rate of 1 kHz or 2 kHz, respectively (XLTEK EMU 128 LTM System). A strip electrode screwed into the frontal bone near the bregma was used as common mode ground and reference. Stimulus-triggered electrical pulses were recorded along with the electrophysiological data for precise synchronization of the stimuli with the neural responses.

Electrode Localization

Computed tomography (CT) scans following electrode implantation were coregistered to the preoperative MRI using iPlan Stereotaxy software (BrainLAB) to determine electrode positions. The three-dimensional brain image thus mounted with electrode locations was normalized to Talairach coordinates (Talairach and Tournoux 1988) and rendered in BrainVoyager software in two dimensions as a surface mesh, enabling precise localization of the electrodes both with relation to the subject's anatomical MRI scan and in standard coordinate space. For joint presentation of all participants' electrodes, locations were projected onto a cortical reconstruction of a healthy subject from a previous study. Given the large number of electrodes and in order to facilitate the data presentation, we subdivided the electrodes into groups based on rough anatomical considerations (see Fig. 9, bottom). It should be emphasized that these subdivisions were approximate since no independent functional delineation based on fMRI was available in these patients. Each electrode was attributed to one of seven regions: low visual, high visual, parietal, auditory, somatosensory, motor, and frontal. Low visual regions included early, retinotopic visual areas, that are at low order in the visual hierarchy, while high visual refers to downstream, category-selective cortical regions that are at high levels in the visual hierarchy (Fig. 9, bottom).

Table 1. Clinical information of the patients

Patient ID	Sex	Age	Handedness	Seizure Localization	Implanted Hemisphere	No. of Usable Electrodes	Sampling Rate, Hz
CL	Female	22	R	Left O	L	126	2,000
DC	Female	35	R	Left F-T	Bilateral	126	2,000
EK	Female	22	L	Left T	L	112	1,000
RS	Male	21	R	Right F-T	R	126	2,000
TD	Female	21	R	Right O	R	104	1,000
WS	Male	44	R	Left F-P	L	126	2,000

R and L are right and left, respectively; O, F, T, and P are occipital, frontal, temporal, and parietal, respectively.

Visuomotor Task

Pictures of faces of both sexes (Minear and Park 2004) were presented followed by a delay interval of 1.5- to 4-s duration terminated by an auditory cue (beep sound). Upon hearing the cue, patients were instructed to press a button to indicate whether the preceding picture was of a man or a woman. Baseline time window for each trial is defined as 500 ms before visual stimulus onset and activation time is 150 until 650 ms after stimulus onset, excluding the trigger execution period.

Object Recognition Task

The patients viewed gray scale digital photographs of faces, man-made tools, buildings, and geometric patterns, which were superimposed with a small white fixation dot. The images were presented for 250 ms in pseudorandom order at a rate of 1 Hz, while the patients performed a 1-back memory task (i.e., pressing a mouse button each time a specific image repeated twice in a row). Stimulus repetitions were infrequent ($\sim 10\%$ of the trials) and were mainly used to keep the patient alert.

Data Analysis

All data analyses were performed using custom-written MATLAB (R2014b) programs (Mathworks).

Preprocessing

Each electrode was rereferenced by subtraction of the averaged signal of all the electrodes, thus discarding nonneuronal contributions (Privman et al. 2007). The 60-Hz frequency line noise and its harmonics were removed with Butterworth bandstop filter (MATLAB, butter). Loose electrodes were identified by spectrograms and were removed (up to 5 electrodes per patient). The patients did not experience epileptic seizures during the recordings; however, an additional preprocessing stage was completed and the trials which were suspected to be contaminated by interictal epileptic discharges (IEDs) were removed and the data reanalyzed (see Table 3). In addition, we defined pathological channels by using IED detection algorithm (Janca et al. 2014), which was shown to be more objective and superior to human detection. The algorithm adaptively models statistical distributions of signal envelopes and enables discrimination of signals containing IEDs from signals with background activity. Irrespectively to task-defined trials, the electrodes that showed IEDs rate higher than algorithm's false positive rate of 8.5 IEDs/min (the IED detected by algorithm but not by human reader) were defined as pathological ($n = 64$, of 720 total) (for details and code, see Janca et al. 2014).

Spectral Analysis

Power spectral density (P_{raw}) was estimated by multitaper method (Thomson 1982). To achieve spectral resolution similar to CGSA (see below), each time interval, T seconds length, was divided to two nonoverlapping windows. We used orthogonal Slepian tapers ($n = 5$, $T/2$ length) to minimize spectral power leakage. The tapers were generated with discrete prolate spheroidal sequences function (dpss, MATLAB). The signal was zero mean and projected onto each taper, padded with zeros to T length (Thomson 1982) and the discrete Fourier transform (\mathcal{F}) was computed by FFT algorithm (MATLAB) and multiplied by its conjugate to produce the power spectrum. For each trial, the power spectrum was averaged over two nonoverlapping windows and tapers. The spectral resolution achieved was $1/T : 2$ Hz for 0.5-s intervals and 1 Hz for 1-s intervals.

$1/f^\chi$ Component Extraction

We used coarse-graining spectral analysis (CGSA) by Yamamoto and Hughson to extract the $1/f^\chi$ components of the spectrum (He et al. 2010; Yamamoto and Hughson 1993). Briefly, the method is based on the scale-invariance property of $1/f^\chi$ signal: it will retain its power when rescaled in time and cross-correlated with the original, nonrescaled time course. In contrast, rescaling in time of harmonic components causes a complete loss of spectral power when cross-correlated with the original.

To obtain the $1/f^\chi$ component we used the following algorithm.

1) Cross-spectrum S_{xx_2} was computed between the signal where each second sample was taken, x_2 (contracted in time by factor of 2 and resulted in $T/2$ length), and the raw signal x_1 : $S_{xx_2} = \mathcal{F}(x_1)\mathcal{F}(x_2)$. The procedure was conducted for odd and even samples, which were used for cross-spectrum with first and second x_1 halves. The signal contraction constrained the spectral resolution to 2 Hz for 500-ms intervals.

2) Cross-spectrum $S_{xx_{1/2}}$ was computed between the signal where each sample was duplicated $x_{1/2}$ (dilated in time by factor of 2) and the raw signal x_1 : $S_{xx_{1/2}} = \mathcal{F}(x_1)\overline{\mathcal{F}(x_{1/2})}$

3) Corrected $1/f^\chi$ power was computed as $P_{1/f} = \sqrt{\|S_{xx_2}\| \cdot \|S_{xx_{1/2}}\|}$.

The rescaling in time in both *directions* 1 and 2 is necessary to correct for arbitrary chosen rescaling factor of 2 (see Yamamoto and Hughson 1993 for details). All the time series components were projected first on the Slepian tapers and cross/auto spectrum results were averaged over tapers (similarly to the raw power spectrum estimation).

Permutation Test

The samples from two sets were randomly divided into two new sets regardless of their labels; the mean difference between two sets was computed across $k = 1,000$ permutations. The P value was estimated as the probability of the mean difference computed on random groups to differ from the original groups.

Raw Power Modulation

The significance of the raw power stimuli-induced modulation was assessed by a random permutation test for the power values in each frequency bin (2 Hz width) defined by spectral analysis in a range of 10–100 Hz (alpha = 0.05, Bonferroni corrected for number of bins).

$1/f^\chi$ Component Linear Model

The linear model for $1/f^\chi$ component of each trial was estimated by iteratively reweighting the least squares with the bisquare weighting function (MATLAB, robustfit), and the exponent χ was extracted. The fraction of variance explained was computed as $[1 - (\text{var}_{\text{err}}/\text{var}_{\text{tot}})]$, where var_{err} is the variance of linear model errors and var_{tot} is the total variance. The difference between $1/f$ scaling exponents during activation and baseline, $\chi_{\text{base}} - \chi_{\text{act}}$, is termed “rotation.” Significance levels of rotation for each electrode were assessed by a paired t -test ($\alpha = 0.05$, Bonferroni corrected). Intersection frequency is the frequency value of the intersection point between the $1/f^\chi$ functions fitted during visual activation and baseline. For each electrode we computed the estimation of the probability density function (PDF) of intersection frequency distribution; its peak value represented the intersection frequency of the electrode. The PDF was estimated by kernel smoothing using normal kernel function (MATLAB, ksdensity) in the range of 0–1,000 Hz frequencies.

Band-Limited Peak Detection

The peaks were selected on the remaining power components after the $1/f^\chi$ component removal ($P_{\text{raw}} - P_{1/f}$), averaged over trials and

satisfying the following conditions: 1) being a local maximum, and 2) the power was significantly modulated by stimulus (permutation test, see *Raw Power Modulation* above).

Synthetic Peaks

For each trial for electrodes with significant gamma peak we found a maximal point in the gamma range. A mixture of 7 sine waves was generated with the same central frequency and amplitude as of the maximal point. This mixture was added to baseline time course and spectral analysis was applied. The synthetic ~30-Hz wide peaks appeared in the raw power spectrum (see Fig. 8) comparable to peaks in activation trials. Similar analysis was done for electrodes with significant alpha peaks, which decreased upon activation. A sine wave with the same frequency of alpha peak in baseline and amplitude equal to difference between alpha peak in baseline and activation was added to activation trials.

RESULTS

ECOG signals were recorded from six patients implanted with 104–126 electrodes for clinical purposes, 720 in total (Table 1). Patients performed two tasks: a visuomotor task and an object recognition task. The visuomotor task included a brief presentation of faces of both sexes for 250 ms, followed by a blank interval presented for a random duration (1.5–4 s), terminated by an auditory cue (Fig. 1A). The participants were instructed to focus on the fixation cross and identify the sex of a face by pressing a button following the auditory cue. The anatomical distribution of electrode sites detected by post implantation CT and MRI scans (see MATERIALS AND METHODS) covered a substantial cortical territory (Fig. 1B). Finally, to expand the analysis to additional visual categories, we used the data from a one-back object recognition memory experiment where images of faces, patterns, houses, and man-made objects were presented (see MATERIALS AND METHODS).

To examine spectral changes associated with the visual response in the visuomotor task, we analyzed separately two time windows: a baseline period extending 500 ms prior to the visual stimulus presentation, and an activation period lasting from 150 ms until 650 ms after the stimulus onset, consistent with known response latencies to faces and to reduce adaptation effects (Fisch et al. 2009) (see Fig. 1C). The intertrial period was not constant, thus reducing expectation effects during the baseline time window. The onset of higher frequency activity in single trials and the event-related potential (ERP) onset both correspond to the activation window onset (Fig. 1C).

Spectral Components: $1/f^\chi$ and Band-Limited Peaks

Conventional spectral analysis included spectrograms showing relative power changes over time, averaged over trials (Fig. 2A, first column). Typical visual responses showed an increase in power across a broad range of high frequencies, compatible with previous findings (Fisch et al. 2009). The average relative power of the activation time window normalized by baseline (Fig. 2A, second column) showed a high-frequency spectral peak. The relative power, however, is showing only a partial picture of spectral response, and it is not clear what transformation was applied to the baseline that leads to the activation spectrum. Therefore, a more comprehensive view of the broadband power modulation can be obtained by visual inspection of the raw power spectrum

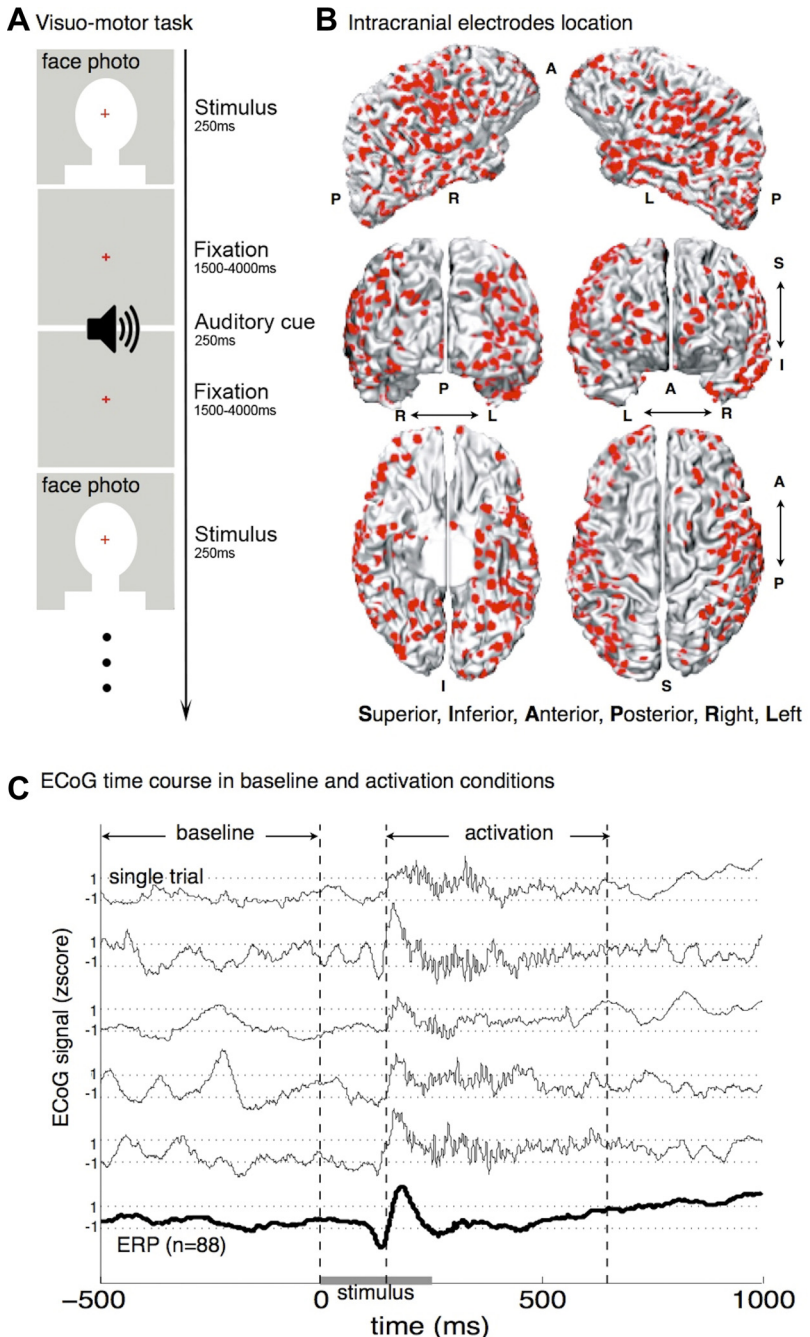


Fig. 1. Experimental setup. *A*: the sequence of a visuomotor paradigm: an image of a face was presented for 250 ms, followed by a random-time (1.5–4 s) blank interval followed by an auditory cue. The task was to identify the sex of a face, by pressing a button on auditory cue. Eighty-eight trials were presented to each patient. *B*: recording sites locations (red points) were obtained from CT and MRI scans of each subject, superimposed on a single subject cortical reconstruction for group analysis (see MATERIALS AND METHODS). *C*: baseline and activation ECoG signals were selected from the recorded time course (baseline: 500 ms prior stimulus onset; activation: 150–650 ms after stimulus onset). The raw data from 5 single trials are shown (thin lines) and the event-related potential (ERP) is shown below in a thick line, averaged over 88 trials recorded from one electrode.

during the baseline vs. activation (Fig. 2*A*, third column). Comparing these raw power spectra revealed three consistent phenomena, which will be quantitatively described in the next sections:

1) $1/\alpha$ spectrum. The raw power spectrum could be approximated by a straight line on a double-logarithmic scale in a broad frequencies range (10–100 Hz) following previous findings (Dehghani et al. 2010; He et al. 2010; He 2014; Miller et al. 2009; Milstein et al. 2009).

2) χ reduction upon activation. The slope of the approximated power-spectrum line was smaller on activation. We describe this broadband phenomenon as counter-clockwise “rotation” of the log-log activation spectrum relative to baseline.

3) Band-limited peak modulations. An increase in band-limited power, superimposed on the $1/\alpha$ spectrum, appeared as a peak centered around frequencies of 80–120 Hz, particularly during the activation condition.

Figure 2*C* illustrates these three characteristics of the ECoG spectral response.

Separation Between the $1/\alpha$ Spectral Component and the Band-Limited Peaks

In order to quantitatively analyze the broadband activity changes, we first separated the $1/\alpha$ component from the band-limited peaks superimposed on it. To extract the $1/\alpha$ in a robust manner, we used the coarse graining spectral analysis (CGSA) introduced by Yamamoto and Hughson (Yamamoto and Hugh-

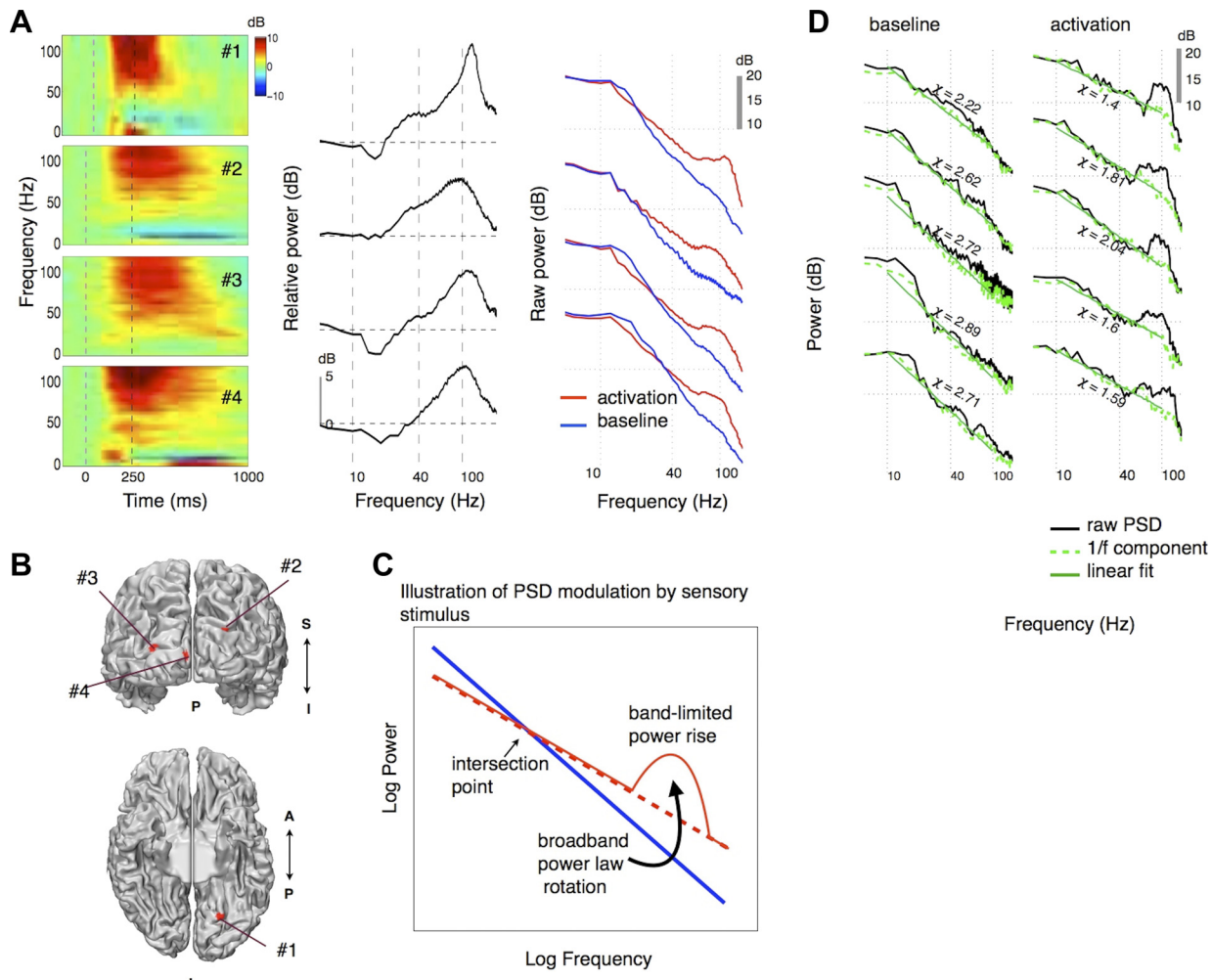


Fig. 2. ECoG data and spectral analysis. *A*: spectral analysis for 4 electrodes located in visual cortex. The first column shows spectrograms averaged over trials ($n = 88$, normalized by prestimulus 250 ms). The second column is a relative power (power in activation window normalized by power in baseline) on a double-logarithmic scale, which demonstrates the broadband frequencies power increase. The third column shows the raw power spectra on log-log scale for activation and baseline windows and includes broadband and band-limited responses. *B*: location of the electrodes presented in *A*. *C*: illustration of the stimuli-induced spectral modulation depicts the activation power spectrum (red solid) and the baseline power spectrum (blue solid) on a log-log scale; see the exponent decrease in the $1/f^{\chi}$ component (red dashed) and the band-limited power increase. *D*: single trials spectral analysis for corresponding baseline and activation time windows (time courses are shown in Fig. 1C). Raw power spectra are shown in black solid line, $1/f^{\chi}$ component in green dashed line. The exponents, χ , were estimated by a linear fit of the $1/f^{\chi}$ component on a log-log scale in 10- to 100-Hz range (green solid line).

son 1993) and utilized in neuroscience (He et al. 2010; Pereda et al. 1998; Valencia et al. 2012). This method does not take prior assumptions on the signal and extracts the $1/f^{\chi}$ components if any are present; therefore, we could separate the band-limited peaks that could interfere with the exponent estimations (see MATERIALS AND METHODS). Since the ECoG signal was already shown to follow a $1/f^{\chi}$ spectrum (for review, see He 2014), the important question explored here was whether the exponent of this approximation remained unchanged or was affected by the sensory-motor response.

To that end the exponent was estimated from the $1/f^{\chi}$ component in the 10- to 100-Hz frequency range for each trial during the baseline and the activation time windows (see Fig. 2*D* and MATERIALS AND METHODS). The frequency range of 10–100 Hz was chosen because of the relatively short (500 ms) duration of our signal sampling window and the possible distortion at <10 Hz frequencies. The 100-Hz limit was chosen since possible action potentials contamination from nearby neurons was reported at higher than 100 Hz frequencies

(Schomburg et al. 2012). Note that the exponent remarkably decreases in the activation condition and the band-limited peaks on top of the $1/f^{\chi}$ component could be observed in the raw power spectrum (Fig. 2*D*).

Exponent Decrease Is Induced by Visual Stimuli in Visual Cortex Electrodes

We tested all electrodes ($n = 720$) for significant stimuli-induced exponent change (either positive or negative) throughout the cortex (paired *t*-test, $P < 0.05$, Bonferroni corrected). We found 80 electrodes with a significant exponent decrease upon activation ($\chi_{\text{base}} - \chi_{\text{act}} > 0$, Fig. 3). This robust phenomenon was evident in single trials (Figs. 2*D* and 3*B*) and electrode averages (Fig. 3*B*). The electrodes that showed visual stimuli-induced exponent modulation were located mostly in the visual cortex (Fig. 3*C*). Only a small minority of electrodes (1% from $n = 720$ total) was found with opposite small-magnitude rotation (exponent

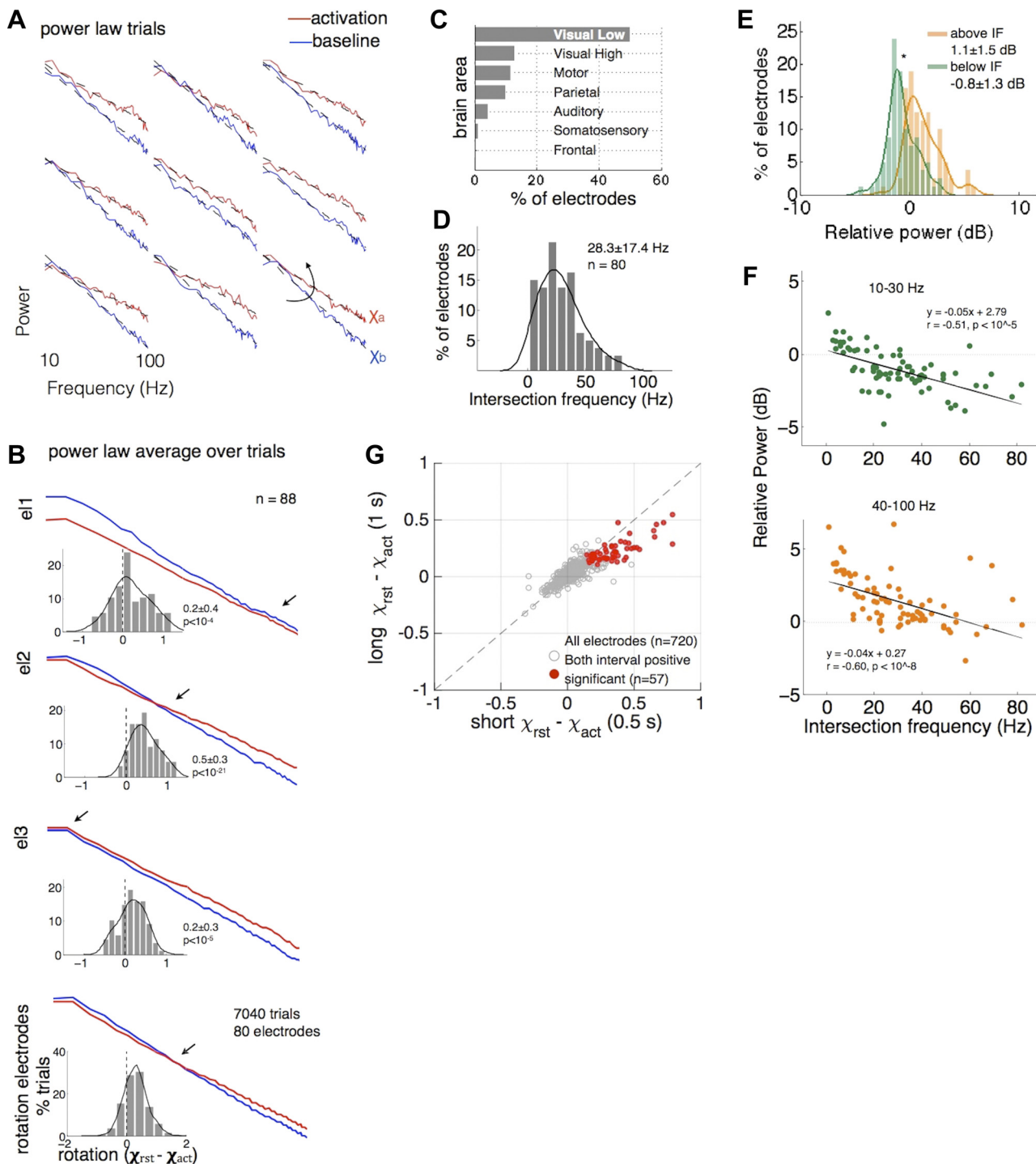


Fig. 3. $1/\chi^{\alpha}$ exponents are modulated by visual stimulus. *A*: $1/\chi^{\alpha}$ components for 9 example trials for one electrode with significant exponent modulation shown at 10- to 100-Hz frequency range (red = activation, blue = baseline, black dashed line = linear fit). *B*: example of $1/\chi^{\alpha}$ component averaged over trials for 3 electrodes (88 trials) and all the trials average for electrodes with significant exponent decrease ($n = 80$). Different intersection points are possible (see arrows). The difference between the baseline and activation exponents are shown in insets. *C*: bar plot of percentage of electrodes with significant exponent decrease ($n = 80$) in each brain area relative to all electrodes implanted in that area. The highest percentage of electrodes with significant rotation was in low-visual areas. *D*: distribution of intersection frequencies ($28.3 \pm 17.4 \text{ Hz}$, $\mu \pm \sigma$). *E*: distribution of raw power modulation above and below the intersection frequency (IF). The power at higher frequencies than intersection point is increasing relative to baseline ($1.1 \pm 1.5 \text{ dB}$, $P < 10^{-8}$) while the power below is decreasing ($-0.8 \pm 1.3 \text{ dB}$, $P < 10^{-5}$). *F*: mean relative power in 10- to 30-Hz range (top panel) and 40- to 100-Hz range vs. the intersection frequency. The higher was the intersection frequency, the bigger was the deviation from baseline (reduction) in low frequencies, while the opposite was true for the high frequencies, where the increased power was diminished at high intersection frequencies. *G*: rotation estimated in long (1 s) vs. short (0.5) intervals for all electrodes (gray). Significant positive rotation was found in 57 electrodes for both interval lengths (paired *t*-test, $P < 0.05$, Bonferroni corrected).

increase, Table 2). In Fig. 3B it is evident that the intersection point between the baseline and activation $1/f^\alpha$ component, which indicates the frequency where the power remained constant during visual activation, could vary between electrodes.

Furthermore, as is shown in Fig. 3F, there was a consistent relationship between activation level (reflected in gamma power increase) and the location of the intersection point. More specifically, with higher gamma the frequency of the intersection point shifted to lower values. The full distribution of intersection frequencies was skewed toward the low frequencies (28.3 ± 17.4 Hz, $\mu \pm \sigma$, Fig. 3D); therefore as a result of the exponent decrease, the power above the intersection frequency increased, while the power below decreased upon activation (Fig. 3E). The values of exponents averaged over trials were in the range of 1.6–3.2, consistent with the values previously reported in ECoG studies (He et al. 2010; Miller et al. 2009). The exponent decrease was found in all patients and the average number of electrodes per patient was 13.4 ± 6.4 electrodes ($\mu \pm \sigma$, $n = 6$). The differences in number of electrodes were expected because of the different electrodes coverage, which was determined solely by clinical needs.

To verify possible spectral analysis edge effects, we tested the exponent modulation using only 1st- and 2nd-order symmetrical tapers. Of 80 electrodes with significant positive rotation that were found with 5 tapers, 76 were also significant using 2 tapers (paired t -test, $P < 0.05$, Bonferroni corrected for number of electrodes, $n = 720$). Only 2 electrodes were significant with 2 tapers but not 5. Next, we

tested the stability of exponent modulation for longer time windows. In this case we reduce the edges differences between activation and baseline trials, but also add a non-active period into the activation window. Therefore, when taking longer intervals, we expect the result to be affected not just by the activation window edge, but also by the short duration (~ 400 ms) of the responses. The baseline and activation windows were defined at 1 s length. Only baseline trials uninterrupted by motor response to previous stimulus were taken into account and only activation windows uninterrupted by the auditory cue. While the rotation magnitude in the 1-s intervals was smaller for most significant electrodes (Fig. 3G) we found significant positive rotation in 57 of 80 electrodes tested on 500-ms intervals (paired t -test, $P < 0.05$, Bonferroni corrected).

We also examined all electrodes with a significant raw power modulation in any frequency in the range of 10–100 Hz ($n = 293$, see MATERIALS AND METHODS). We found a significant average exponent decrease over this population [Fig. 4A, paired t -test, $\chi_{\text{base}} - \chi_{\text{act}} = 0.1 \pm 0.17$ ($\mu \pm \sigma$), $P < 10^{-20}$]. Examining the goodness of linear model (explained variance) of the $1/f^\alpha$ component showed remarkable levels of $96.5 \pm 1.2\%$ and $96.4 \pm 1.3\%$ ($\mu \pm \sigma$) for activation and baseline, respectively (Fig. 4B and MATERIALS AND METHODS). The histogram of frequencies with significant raw power increases and decreases over the entire population of electrodes (Fig. 4C, permutation test, see MATERIALS AND METHODS) reveals that the frequency which showed the minimal change in power upon activation centered around ~ 35 Hz (arrow).

Table 2. Average responses

Effect on Activation	VIS	VIS Face	VIS Pattern	VIS House	VIS Object	AUD	MOT
<i>1/f component</i>							
No. of electrodes, χ decrease	80	56	17	47	36	48	79
No. of electrodes, χ increase	10	0	0	1	0	1	4
Rotation $\chi_{\text{base}} - \chi_{\text{act}}$	0.31 ± 0.1	0.38 ± 0.2	0.52 ± 0.2	0.48 ± 0.2	0.45 ± 0.1	0.25 ± 0.1	0.1 ± 0.16
Intersection frequency, Hz	28.3 ± 17.4	27.7 ± 13.2	28.4 ± 9.9	26.3 ± 10.6	29.3 ± 12.9	42.4 ± 20.1	59.3 ± 25.7
Main location	Low visual	Low visual	Low visual	Low visual	Low visual	Motor Auditory	Motor Somatosensory
<i>Gamma</i>							
No. of electrodes with peak	42	23	21	29	23	6	6
Peak power	0.82 ± 1.02	0.78 ± 0.66	1.02 ± 0.72	0.79 ± 0.57	0.78 ± 0.46	ND	ND
Peak frequency, Hz	87.5 ± 11.7	83.2 ± 9.7	75.6 ± 13.7	80.4 ± 13.9	79 ± 15.6	ND	ND
Main location	Low visual	Low visual	Low visual	Low visual	Low visual	ND	ND
χ_{act} peak corr coeff	$-0.38, P < 0.012$	$-0.61, P < 0.003$	significant		ND		
<i>Alpha</i>							
No. of electrodes peak decrease	72	40	5	23	22	58	57
No. of electrodes peak increase	3	1	0	4	1	2	3
Peak power on activation	40.2 ± 50.4	20.2 ± 19.5	ND	13 ± 11.4	31.6 ± 37.9	29.1 ± 25.3	27.9 ± 22.5
Peak frequency, Hz	11.7 ± 0.9	11.3 ± 1.2	ND	10.8 ± 1.6	10.7 ± 1.7	11.8 ± 0.9	11.9 ± 0.3
Main location	Low visual	Low visual	ND	Low visual	Low visual	Motor Somatosensory	Motor Somatosensory
χ_{act} peak corr coeff	$0.51, P < 10^{-5}$	$0.62, P < 10^{-4}$	ND	Not significant	$0.60, P < 0.005$	$0.65, P < 10^{-7}$	$0.3, P < 0.05$

Values are means \pm SD. VIS, visual responses to faces in visuomotor experiment and categories in object recognition (face, patterns, houses, and objects); AUD, responses to auditory cue; MOT, responses to button press; ND, not enough responsive electrode available, $n \leq 6$.

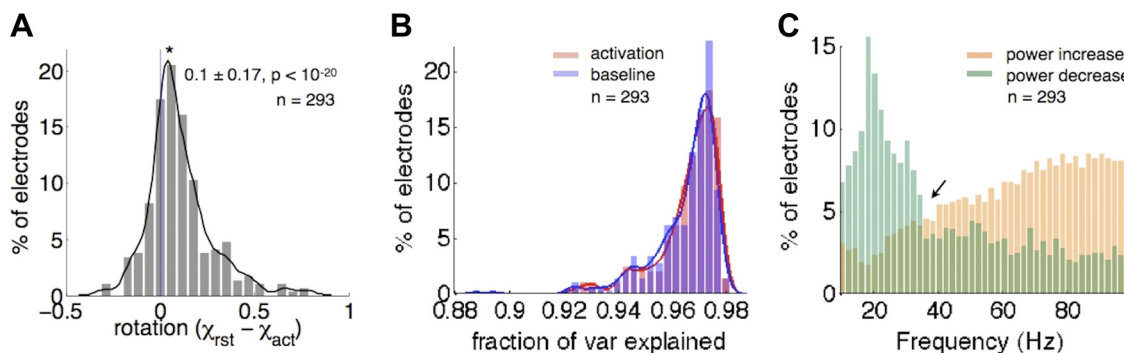


Fig. 4. $1/f^x$ component analysis in electrodes with raw power modulation. *A*: the mean rotation ($\chi_{rst} - \chi_{act}$) distribution of all electrodes with any power modulation ($n = 293$) was significantly different from zero (one-sample t -test, $P < 10^{-15}$). *B*: distribution of variance explained for electrodes in activation ($96.5 \pm 1.2\%$, $\mu \pm \sigma$) and baseline ($96.4 \pm 1.3\%$, $\mu \pm \sigma$) for all electrodes with power modulation ($n = 293$). *C*: distribution of frequencies where the power significantly increased (red) or decreased (blue) for all electrodes with power modulation ($n = 293$). The trough (see arrow) is located at around 35 Hz, which is related to average intersection frequency.

The $1/f^x$ Component Across Various Visual Categories, Auditory Cues, and Button Presses

To further confirm these results and examine whether the exponent modulation could be generalized to other visual categories we examined the ECoG responses during the object recognition experiment. In this task, images of faces, patterns, houses, and man-made objects were presented (see MATERIALS AND METHODS). The baseline and activation windows for the visual responses were defined identically to those used for the visuomotor experiment. The exponent decreased in 56, 17, 47, and 36 electrodes for each category, respectively, and these electrodes were mostly located in low visual areas as expected (see Table 2 and Fig. 5). The mean intersection frequency value was ~ 30 Hz for different visual categories, similarly to visual responses in visuomotor tasks (see Table 2 and Fig. 5).

The $1/f^x$ component analysis was applied also to the auditory cue responses and the button presses. In the visuomotor experiment, the participants' task was to identify the sex of a face by button press when they heard an auditory cue; thus we expected the involvement of motor neural response even though the trials were locked to the auditory cue. For auditory responses we defined an activation window lasting from 100 to 600 ms after the auditory cue onset and a baseline window as 500 ms prior the auditory cue onset. We tested all electrodes for exponent change and found 48 electrodes with exponent decrease and 1 electrode with increase (Table 2). The rotation amplitude was smaller than that found in visual responses and the intersection frequency was higher (~ 40 Hz, Table 2, Fig. 5A). For button press we chose the same baseline time window as for the auditory cue; the activation window was for 500 ms

starting at the button press onset. We found 79 electrodes with exponent decrease (Table 2), which were located mostly at the somatosensory and motor cortices (Fig. 5B). The intersection frequency was even higher for button press responses, ~ 60 Hz.

Signal Artifacts Control Analyses

ECoG signals were carefully searched in each electrode for possible epilepsy-related or other artifacts. Each electrode's ECoG time course was inspected for interictal epileptiform events. All suspected trials were rejected and all the data were reanalyzed. The results were nearly identical to the raw data results (see MATERIALS AND METHODS and Table 3). We therefore opted to show the raw data in the previous analysis. We have also defined the pathological channels with the IED automatic detector (see MATERIALS AND METHODS and Janca et al. 2014) and found that only a minority of electrodes with significant rotation showed IED-defined pathological activity ($n = 2$ for visual, $n = 5$ for auditory, and $n = 9$ for button press conditions).

Band-Limited Peaks Superimposed on Top of the $1/f^x$ Component

Next, we analyzed the band-limited peaks in power beyond the $1/f^x$ spectra that were computed by subtraction of the $1/f^x$ component from the raw spectra (Yamamoto and Hughson 1993). The peaks were defined as local maxima where the power was also significantly modulated by the visual response (see MATERIALS AND METHODS and Fig. 6A). We found 42 (from $n = 720$ total) electrodes with significant gamma peak that

Fig. 5. $1/f^x$ exponents are modulated by different sensory stimuli. *A*: average intersection frequency for electrodes with significant exponent modulation in object recognition experiment as response to face (blue, $n = 56$), pattern ($n = 17$), object ($n = 36$), and house ($n = 47$) visual stimuli and as response to button press (green, $n = 79$) and auditory cue (green, $n = 48$). The error bars represent SE. No significant difference was found between visual categories; for button press the intersection frequency was the highest and for auditory cue it was higher for all categories except patterns [one-way ANOVA, $F(5,277) = 32.05$, $P < 10^{-25}$, post hoc Tukey HSD test, see Table 2 for $\mu \pm \sigma$]. *B*: anatomic location for electrodes in *A*, given by percentage of electrodes with significant exponent modulation relative to all electrodes implanted in that region (same color code as in *A*).

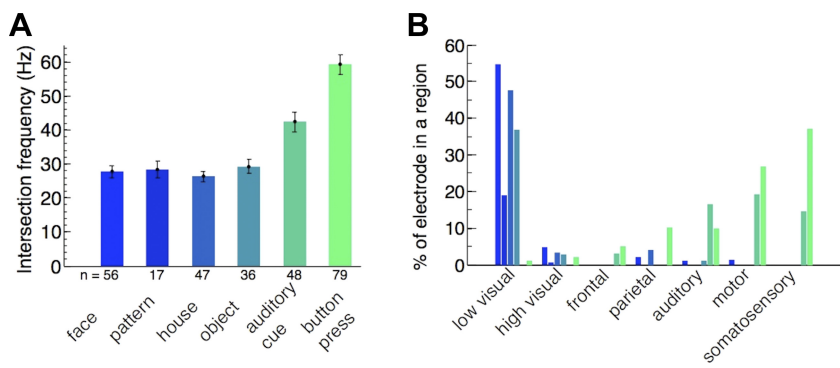


Table 3. Average responses after epileptic artifacts rejection

Effect on Activation	VIS	VIS Face	VIS Pattern	VIS House	VIS Object	AUD	MOT
<i>1/f component</i>							
No. of electrodes, positive rotation	74	56	15	46	36	42	75
No. of electrodes, negative rotation	9	0	0	1	0	2	3
Rotation $\chi_{base} - \chi_{act}$	0.33 ± 0.15	0.38 ± 0.2	0.52 ± 0.2	0.48 ± 0.2	0.45 ± 0.1	0.26 ± 0.1	0.33 ± 0.18
Intersection frequency, Hz	28.2 ± 18.8	27.7 ± 13.2	29.1 ± 10.4	26.2 ± 10.7	29.3 ± 12.9	43.7 ± 15.7	60.3 ± 26.1
Main location	Low visual	Motor auditory	Motor somatosensory				

Values are means \pm SD. VIS, visual responses to faces in visuomotor experiment and categories in object recognition; AUD, responses to auditory cue; MOT, responses to button press.

centered around 90 Hz [87.5 ± 11.7 Hz ($\mu \pm \sigma$), Fig. 6A, inset].

The height of the gamma peak in these electrodes was significantly correlated to the average relative power in the gamma range (Fig. 6B). In contrast, the correlation between peak height and peak frequency was not significant, which is comparable to a recent study in monkeys (Jia et al. 2013). As expected, due to the correlation between relative gamma power and gamma peak, the electrodes with gamma peaks were located mostly in the visual cortex (Fig. 6D). We found also 72 electrodes with significant decrease in the alpha peak [11.7 ± 0.9 Hz ($\mu \pm \sigma$)] upon activation (Table 2); the difference between alpha peaks in baseline and activation conditions was correlated to relative power in alpha range (Fig. 6C). These electrodes were located mostly in low-order visual areas (Fig. 6E). The gamma peaks were found in 7 ± 7.3 electrodes and alpha peaks in 12 ± 6.4 electrodes per patient ($\mu \pm \sigma$, $n = 6$). The differences in number of electrodes were expected because of the different electrodes coverage, which was determined solely by clinical needs.

Similar results were found for the different categories in the object recognition experiment, except the “patterns” condition (see MATERIALS AND METHODS) where only 5 electrodes had alpha peak decrease (Table 2 and Fig. 7). The electrodes with

alpha and gamma peaks were located mostly in the visual cortex. In the responses for auditory cue and button presses, we found 57 and 58 electrodes with significant modulation of the alpha peaks beyond the $1/f^\alpha$ component (Table 2) but only 6 electrodes with a significant gamma peak. Most electrodes with a significant modulation of the gamma peak or the alpha peak were located at the auditory, somatosensory, and motor cortices, as expected (Table 2).

Control Analyses for Potential Band-Limited Peak Artifacts

It could be argued that the reduction we found in the $1/f^\alpha$ exponent was merely a consequence of the emergence of the band-limited gamma peaks during activation. If this were the case, the $1/f^\alpha$ component would be contaminated by the strong band-limited gamma increase during activation, leading to apparent reduction in exponent levels. One argument against this possibility relates to the goodness of fit for baseline and activation $1/f^\alpha$ components. Distortion of the activation $1/f^\alpha$ component induced by the band-limited power changes should be expected in the range of 60–100 Hz, leading to reduced fit, if there were a substantial “leakage” from the band-limited bumps onto the linear $1/f^\alpha$ component. We examined the electrodes for a difference in goodness of fit between baseline

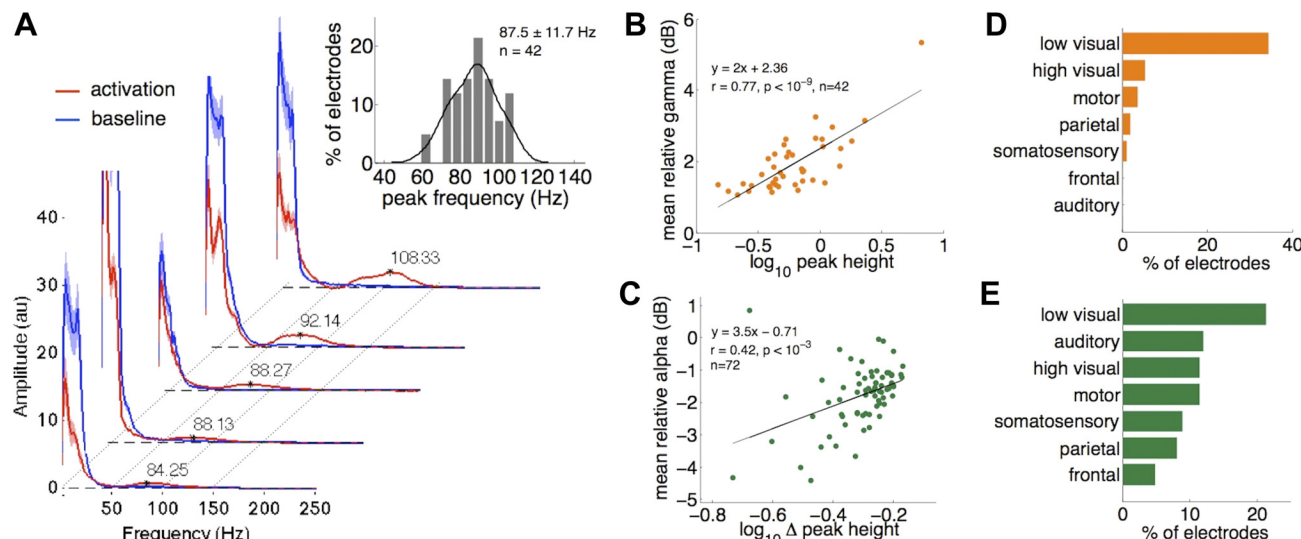


Fig. 6. Band-limited power was modulated during visual response. A: the residual power after $1/f^\alpha$ component removal is shown for 5 electrodes averaged over trials, for baseline (blue) and activation (red) conditions. The band-limited peaks are visible in the alpha and the gamma range, and their frequency value is shown. Distribution of peak frequencies in the gamma range is shown in inset. B: mean relative gamma power and band-limited peak heights were correlated. C: mean relative alpha power and difference between alpha band-limited peaks heights in baseline and activation were correlated. D: bar plot of percentage of electrodes with a band-limited gamma peak in each brain area relative to all electrodes implanted in that area. The highest percentage of electrodes is located in low-visual areas. E: bar plot of percentage of electrodes with a decreased band-limited alpha peak in each brain area relative to all electrodes implanted in that area. The highest percentage of electrodes is located in low-visual areas.

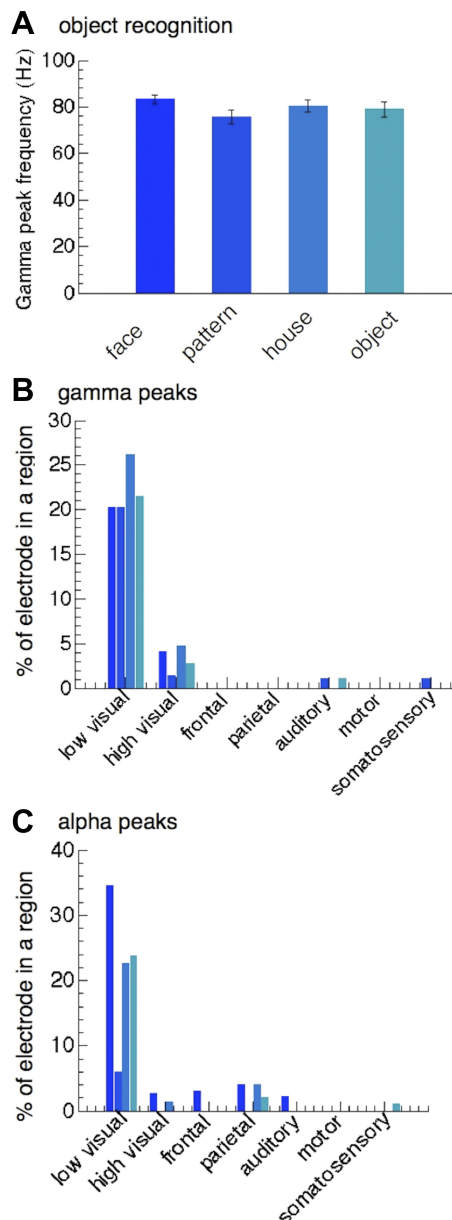


Fig. 7. Band-limited power modulation in object-recognition experiment. **A:** gamma peak frequency was ~80 Hz for different visual categories: face ($n = 23$), pattern ($n = 21$), house ($n = 29$), and object ($n = 23$); error bars for SE. No significant difference was found between categories [one-way ANOVA, $F(3,102) = 1.58$, $P = 0.19$, see Table 2 for $\mu \pm \sigma$]. **B:** anatomic location of electrodes with emerged gamma peak given by percent of electrodes with significant gamma peak relative to all electrodes implanted in that area. Most electrodes were located at low visual areas. **C:** same as **B** but for electrodes with significant alpha peak decrease.

and activation trials specifically in the range of 60–100 Hz, where the harmonic amplitude changes occurred. We found only 6 electrodes with a significant fit difference between baseline and activation (permutation test, $P < 0.05$, Bonferroni corrected for number of tested electrodes, $n = 720$). The goodness of fit was better in activation condition in 1 electrode. The goodness of fit was better in baseline condition in 5 electrodes, but only one of these electrodes showed a significant gamma peak and rotation.

A second argument against the possibility that the exponent change was a consequence of the band-limited peaks modula-

tions is the finding that a significant exponent change was observed even in electrodes showing no such changes. We found electrodes that showed a significant rotation but no gamma peaks ($n = 41$) and a significant rotation but no significant alpha peak decrease ($n = 50$).

Finally, a simulation was conducted specifically aimed at ruling out the possibility of slope contamination by the gamma peaks as follows. Based on the power spectra during baseline derived from all electrodes with a significant gamma peak and rotation ($n = 39$), a “synthetic” sensory-driven power spectra simulation was generated. This simulated power spectra was constructed by adding a mixture of sine waves simulating the gamma “bumps” to baseline time course obtained in the no-stimulus condition (see Fig. 8 and MATERIALS AND METHODS). The location of this synthetic peak was at a similar frequency and with the same amplitude as the maximal point in harmonic power found in the activation trials. Having generated thus an ECoG power spectrum function with band-limited power distortions similar to the sensory responses, we ran our analysis on this simulated “chimera” signal (see Fig. 8A). We defined synthetic rotation as the difference between the exponents of the baseline $1/f^\alpha$ component and the one generated by the synthetic power spectrum. Had the gamma peak caused the rotation, the synthetic rotation should have been similar to the actually measured one. In contrast, we found that the synthetic rotation was drastically smaller than the real one. Thus, while the mean synthetic rotation was $0.06 \pm 0.04 (\mu \pm \sigma, n = 39)$, the real rotation measured was 6.8-fold larger ($0.40 \pm 0.16, \mu \pm \sigma, n = 39$). The difference was highly significant in the vast majority (95%) of electrodes (paired t -test, $\alpha < 0.05$, Bonferroni corrected, $n = 39$). Figure 8B depicts a scatterplot showing the measured exponent rotation derived from the true activated spectra (y-axis) vs. the exponent derived from the synthetic “bump” simulation described above (x-axis). Similar analysis was done for electrodes that showed both a significant decrease in alpha peak and a significant rotation ($n = 30$). The synthetic rotation was $0.09 \pm 0.06 (\mu \pm \sigma, n = 30)$, significantly lower than real measured rotation $0.35 \pm 0.18 (\mu \pm \sigma,$

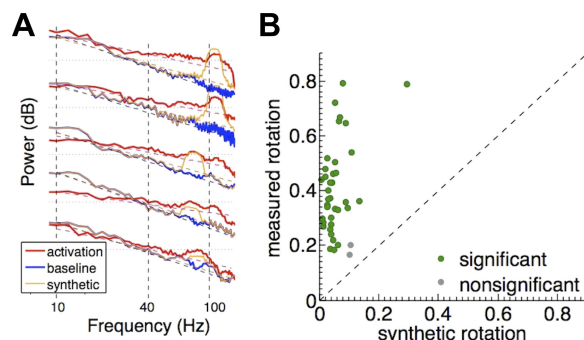


Fig. 8. Band-limited peaks in the gamma range did not affect the rotation. **A:** example of raw spectra for single trials of measured data, baseline (blue) and activation (red). Raw spectra for synthetic trials, which include the synthetic harmonic peak that was added to baseline time course, is shown in orange. The linear model of the $1/f$ component appears in dashed colored lines. **B:** scatterplot of measured vs. synthetic rotation, with dashed unitary line. Measured rotation ($\mu = 0.4$) was computed as the difference in the baseline and activation exponents, averaged over trials. Synthetic rotation ($\mu = 0.06$) is the difference between exponents in baseline and synthetic trials. The exponents were extracted from the $1/f$ component as described in MATERIALS AND METHODS.

$n = 30$) in 27 of the 30 electrodes (90%, paired t -test, $\alpha < 0.05$, Bonferroni corrected).

$1/f^\alpha$ Exponent and Band-Limited Peak Height

Comparing the main components of spectral responses—exponents, band-limited gamma, and alpha peak heights—revealed a significant correlation. The agreement was also evident in the substantial overlap of the spatial locations of the electrodes showing each of these parameter's changes (Fig. 9A). We found negative correlation between the gamma peak height and the exponent during activation ($r = -0.38$, $P < 0.02$) (Fig. 9B) and similar correlation was found in the object recognition experiment for faces, houses, and objects, but not patterns (Table 2). We found a positive correlation between the alpha peak height and the exponent ($r = 0.51$, $P < 10^{-5}$) and a similar correlation for the object recognition

experiment except for the responses to houses (Table 2). For auditory responses and button presses we found a correlation between alpha peak height and the activation exponent value, comparable to the correlation we found in visual responses (Table 2), but we did not have a sufficient number of gamma peaks for similar analysis ($n = 6$). The distributions of the exponents in electrodes with significant alpha and gamma peaks were significantly different (Fig. 9D), where gamma peaks occurred in electrodes with lower exponents on activation.

Next we compared the exponent change in the population of electrodes that had significant exponent change but did not show a significant gamma peak with those that did. Our results show a significant difference in the rotation value ($\chi_{\text{base}} - \chi_{\text{act}}$) of the two populations: 0.17 ± 0.13 ($n = 46$) vs. 0.3 ± 0.2 ($n = 34$) (2-sample t -test, $P < 0.005$), respectively. The

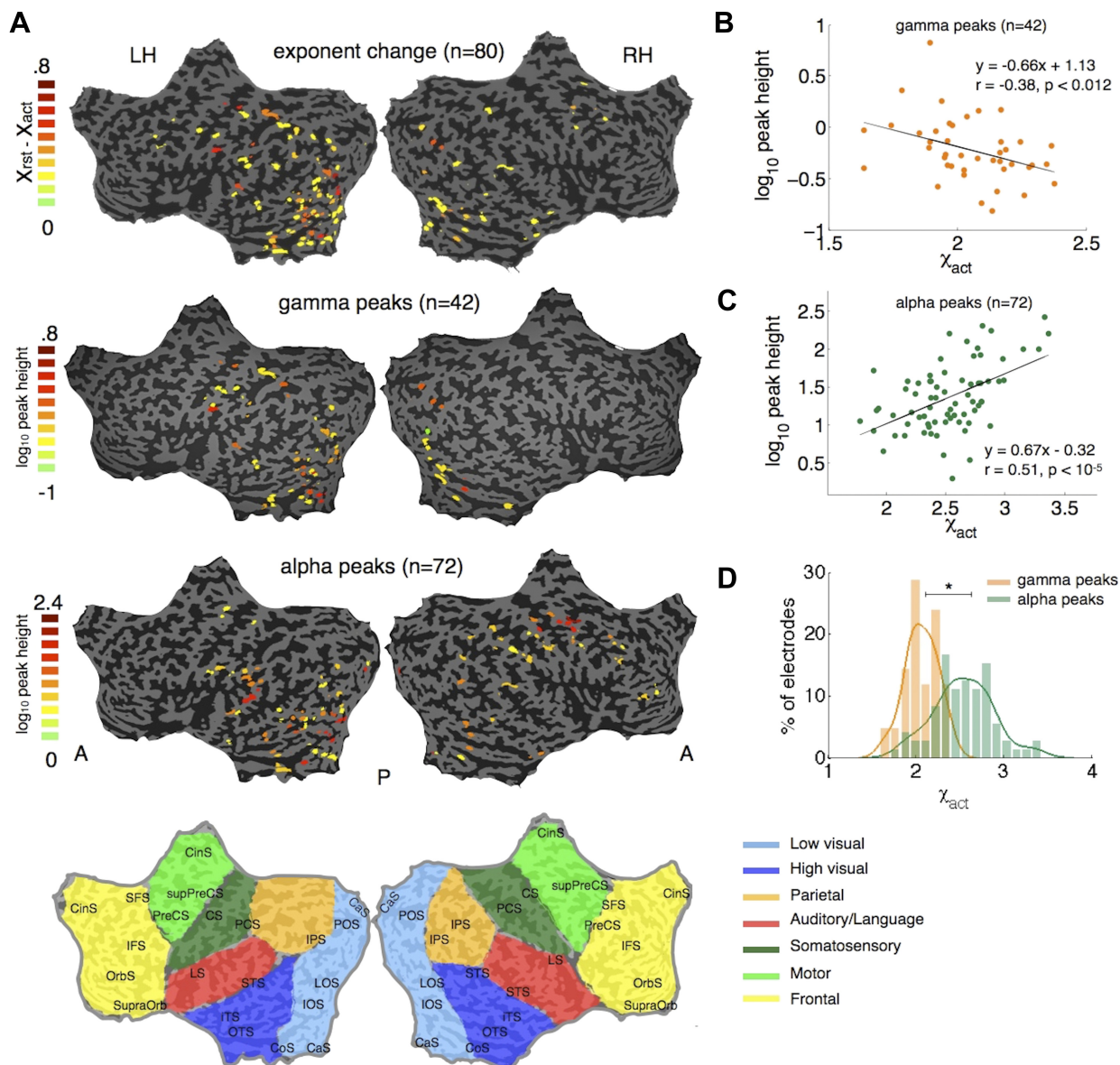


Fig. 9. Band-limited peaks and broadband power relation. *A*: inflated map of the cortex with the electrodes colored by rotation magnitude ($\chi_{\text{rst}} - \chi_{\text{act}}$), and gamma and alpha band-limited peaks heights. *B*: gamma band-limited peak height was significantly correlated to the exponent during activation. *C*: alpha band-limited peak height was significantly correlated to the exponent during activation. *D*: the distributions of exponents of activation window for electrodes with emerged gamma peak (2.05 ± 0.2 , $\mu \pm \sigma$) and electrodes with reduced alpha peaks (2.5 ± 0.3 , $\mu \pm \sigma$) were significantly different (2-sample t -test, $P < 10^{-13}$).

exponents on activation were lower for electrodes with gamma peaks (2.1 ± 0.3 , $n = 34$) than in electrodes with no significant peak (2.5 ± 0.3 , $n = 46$) (2-sample *t*-test, $P < 10^{-7}$). Thus the gamma peaks occurred only in electrodes with largest rotation and lowest exponent on activation.

DISCUSSION

Our analysis of ECoG signals reveals that the complex dynamics of mass neuronal activation is reflected in two main effects: first, a reduction in the $1/f^\alpha$ exponent in the broad range of frequencies of 10–100 Hz (rotation); and second, modulation of band-limited power peaks, i.e., emergence of a peak in high gamma and decrease of the alpha peak amplitude. The band-limited peaks' heights were correlated with the exponent on activation, where the significant gamma peaks emerged in electrodes with lower exponents and higher rotation. These effects were found across the cortex and in responses to various visual categories, auditory and motor activity.

To the best of our knowledge, this is the first study to report a reduction in $1/f^\alpha$ exponent as a consistent signature of neuronal activity in ECoG recordings. We found such exponent change across different cortical areas and tasks. Furthermore, a major advantage of this phenomenon is its dependence on a broad range of frequencies, suggesting it may serve as a reliable and sensitive means to assess neuronal activations in LFP and ECoG recordings.

It could be argued that the exponent reduction we observed was merely an artifact of the specific analysis employed, i.e., the approximation to a $1/f$ function may have suffered from distortions imposed by the high, band-limited gamma peaks that emerge in the activated electrodes. Three results argue against this trivial account. First, if our $1/f$ estimation procedure were inadequate in the face of the gamma peak distortions, we would expect a reduction in the fit of the estimate of the undistorted baseline, compared with the distorted, active state. Only one electrode with both rotation and band-limited gamma peak showed better goodness of fit during baseline than in the activation condition in the range of 60–100 Hz. Second, imposing severe distortions, of similar magnitude both in the gamma peaks generated as well as alpha peak decreases upon activation, in simulated data failed to reproduce the magnitude of exponent changes that could explain the measured rotations (Fig. 8). Finally, significant exponent changes were observed also in electrodes in which no significant gamma distortion was observed ($n = 41$) and similarly, significant rotation was observed in electrodes in the absence of a significant alpha peak decrease ($n = 50$), further confirming that the exponent change was not a direct consequence of the gamma bumps. The results were stable also for the first two symmetrical tapers analysis and for longer intervals of 1 s, thus arguing against a major role for edge effects. Thus we can safely conclude that the exponent reduction is a separate cortical phenomenon that is correlated, but not a direct outcome of the analysis procedure of the band-limited gamma peaks.

Two previous studies examined the possibility of an exponent shift in the ECoG power spectrum during a motor task in patients; however, in contrast to our findings, these studies reported a constant exponent in the 10- to 100-Hz frequency range (He et al. 2010; Miller et al. 2009). The difference may be due to examining power spectra averages, which may not

reflect accurately the power spectra of single trials [$\log \sum_{i=1}^N 1/f^{x_i} \neq \sum_{i=1}^N \log(1/f^{x_i})$]. Alternatively, the difference may be due to longer sampling durations. These differences suggest that the exponent modulation reported here might be a short-lived phenomenon that is compatible with the short time window needed for most neuronal computations (tens to hundreds of milliseconds). He et al. found an exponent decrease in ultra-low frequencies of the spectrum (<0.01 Hz), which was induced by button presses tasks. Unfortunately, our experiments did not allow such long time scales. An additional study tested the modulation in exponents of intracellular recordings in cat's visual cortex *in vivo* (El Boustani et al. 2009). The authors found that the exponent was not constant, but was modulated by the statistics of the presented visual stimuli. We confirm this finding in human extracellular neural population activity and extend it to motor and auditory modalities.

What could be the underlying electrophysiological processes that lead to the observed exponent decrease? Attempting to relate the observed changes to cortical organization, it should be noted that the cortex contains a rich connectivity pattern; thus the spiking activity of groups of neurons is not independent—instead, it is correlated on a range of time scales (Deco et al. 2011; Smith and Kohn 2008). A plausible source of the $1/f^\alpha$ spectrum might be a distribution of these timescales. We found that the exponent decreases during sensory and motor responses, reflecting a shift of power towards higher frequencies. This phenomenon could appear when pairwise cross-correlations occur on shorter time scales during neuronal activation, thus generating faster fluctuations (Abeles 1991; Abeles et al. 1995; Bair et al. 2001; de la Rocha et al. 2007; Gutnisky and Dragoi 2008; Ostojic et al. 2009; Tan et al. 2014). Furthermore, attentional effects, which are likely to be generated during the visual activation period, have been shown to reduce the amplitude of slow fluctuations in neuronal firing (Churchland et al. 2010). Such effect may be reflected in broadband low frequencies and thus further enhance the exponent reduction observed in the power spectra during the visual activation period.

Another possibility could relate the power spectrum to the shape of synaptic potentials. Our analysis suggests that the synaptic potential rise and decay time constants would be shorter upon cortical activation. This process is expected due to the higher membrane conductance levels that are associated with high levels of postsynaptic excitations during neuronal activations (Mitchell and Silver 2003) that will lead to faster membrane potential fluctuations. However, the exact shape of the synaptic potential and its time constants distribution in the human cortex are unknown; therefore its relationship to the power spectrum of population signals remains to be studied.

Miller et al. proposed a model that explains the changes in ECoG signals upon activation as a uniform broadband increase in power spanning all frequency bands, which is concurrently sculpted by a band-limited reduction in power at the alpha-beta range (Miller et al. 2009). The latter effect has been considered a separate mechanism, similarly to the alpha block or the evoked response desynchronization (Crone et al. 1998a) phenomenon. Compatible with this model, our data indeed show a decrease in alpha-beta power concurrently with the gamma power increase. However, we show that in parallel to these frequency-specific changes there was a more uniform effect,

i.e., the exponent change that spanned from the alpha to the gamma bands.

The exponent modulation phenomenon was consistent over modalities; however, the intersection points of the “rotation,” i.e., the frequencies in which no power change was observed upon stimulation which constitute the transition between the task-driven increases and decreases in power, were different: ~30 Hz for visual responses and ~40 Hz and ~60 Hz for auditory and motor, respectively (Fig. 5A, Table 2). The intersection frequency was also inversely related to the increase in gamma power. The intersection point relation to motor behavior was reported by Miller et al. (Miller et al. 2008); however, this phenomenon was hypothesized to originate in uniform power spectrum increase (constant exponent) and separate low-frequencies filtering. Our findings suggest that the phenomenon of alpha block is not a separate mechanism, but rather one component in a process that consists also of a rotation of the $1/f^x$ component or the entire 10- to 100-Hz spectrum, leading to a reduction in power below the intersection frequency and increased power above it (Fig. 3, E and F). Under this formulation, the larger spatial spread of the ERD phenomena compared with the gamma increase (Crone et al. 1998b) may be explained by the larger anatomical spread (including spreading across the skull boundary) of low frequencies compared with the localized nature of high-frequency gamma oscillations. Such differential anatomical spread is likely due to higher signal phase cancellations (due to, e.g., small temporal jitter in signal conduction times) that are expected to occur at high but not at low frequencies over distance. However, more studies are needed to clarify the basis of such differences in spatial spread.

The second task-driven phenomenon we describe is an increase in band-limited power (“peaks”) at a high gamma frequency range and the decrease of a peak in low (alpha) frequencies. Our results are in agreement with previous findings of narrow band gamma increases to the extent that we see, particularly under high exponent changes, a band-limited increase in power (see Figs. 2 and 6). However, in our data, recorded from human cortex, the frequency of this band-limited peak centered around higher gamma frequencies, i.e., 80–100 Hz rather than the 35–85 Hz typically found in monkey and cat studies (Eckhorn et al. 1988; Gray and Singer 1989; Henrie and Shapley 2005). Recently it was proposed, based on recordings in nonhuman primates, that moving from the anesthetized to the awake state causes a shift in the gamma peaks to higher frequencies (Xing et al. 2012), which may partially account for our observed discrepancy. The source of the observed band-limited gamma power increase is not clear. In our analysis it was specific to the cases where the exponent reduction was particularly high. The effect may reflect a sort of “resonance” or synchronization of neurons, comparable to narrow band 40-Hz synchronization (Fries et al. 2001), but shifted to higher frequencies in the human cortex. However, an alternative explanation is spectral leakage of actual spiking activity, which has been shown to contain frequencies in the high gamma range (Scheffer-Teixeira et al. 2013; Schomburg et al. 2012). Finally, a simple network mechanism that could generate a gamma peak effect was proposed in a recent study (Xing et al. 2012) demonstrating that gamma peaks could be well simulated by a simple recurrent excitatory-inhibitory net-

work, implementing essentially a filter that integrates random noise inputs.

Our results reveal a significant correlation between the exponent reduction and the increase in harmonic peak amplitude during the active state. Since, as described above, both these phenomena appear to depend on the level of neuronal activation, the link between the harmonic peak and the exponent change may simply be derived from this common source driving both phenomena. For example, in the modeling work of Xing et al. (Xing et al. 2012) the amplitude of the gamma harmonic peaks strongly depended on the level of inputs to the simulated network. In parallel, higher activity leads to reduced slow fluctuations (Churchland et al. 2010), generating a concurrent reduction in power spectrum exponent. However, since the precise mechanisms that underlie these two phenomena are not fully clarified yet, the source of the link between them remains to be fully elucidated as well.

In our study, we demonstrate a neuronal response that unifies the power modulations across different frequency bands. However, it is important to emphasize that such uniformity does not necessarily rule out the possibility of frequency-specific information transfer as well. For example, Belitski and colleagues examined LFP power spectra recorded from the primary visual cortex of anesthetized macaques (Belitski et al. 2008) and found that the presentation of naturalistic color movies elicited power modulations that conveyed complementary information about the stimuli in low and high frequencies. In our model, the regulation of frequency bands is mediated by an intersection point and an exponent, which can vary on different stimuli and in different electrodes.

It is important to emphasize that our analysis does not rule out the possibility that alternative, more complex, power spectrum function may actually fit the ECoG data better. However, the exponent change provides a straightforward fit to the data and may prove to be a sensitive new means for detecting neuronal activations in ECoG and LFP responses. Furthermore, the correlation found between the changes in exponent and the amplitude of the band-limited peaks suggests the possibility of further functional links between these seemingly separate expressions of neuronal activation.

ACKNOWLEDGMENTS

We thank Prof. M. Abeles for helpful discussions and comments on the manuscript. We thank Dr. M. Ramot for reviewing the manuscript and helping us to improve it. We thank the participants for volunteering to take part in the study.

GRANTS

This work was funded by the EU FP7 VERE, ICORE program (ISF 51/11), HBP flagship grants, and the Helen and Martin Kimmel Award to R. Malach.

DISCLOSURES

No conflicts of interest, financial or otherwise, are declared by the author(s).

AUTHOR CONTRIBUTIONS

Author contributions: E.P., N.N., C.E.S., A.D.M., M.T., and R.M. conception and design of research; E.P. and M.H. analyzed data; E.P., G.C., A.D.M., M.T., and R.M. interpreted results of experiments; E.P. prepared figures; E.P. and R.M. drafted manuscript; E.P., N.N., M.H., G.C., C.E.S., A.D.M., M.T., and R.M. edited and revised manuscript; E.P., N.N., S.B., G.C., C.E.S.,

A.D.M., M.T., and R.M. approved final version of manuscript; S.B. and A.D.M. performed experiments.

REFERENCES

- Abeles M, Bergman H, Gat I, Meilijssen I, Seidemann E, Tishby N, Vaadia E.** Cortical activity flips among quasi-stationary states. *Proc Natl Acad Sci USA* 92: 8616–8620, 1995.
- Abeles M.** *Corticonics: Neural Circuits of the Cerebral Cortex*. New York: Cambridge University Press, 1991.
- Bair W, Zohary E, Newsome WT.** Correlated firing in macaque visual area MT: time scales and relationship to behavior. *J Neurosci* 21: 1676–1697, 2001.
- Bak P, Tang C, Wiesenfeld K.** Self-organized criticality: an explanation of 1/f noise. *Phys Rev Lett* 59: 381–384, 1987.
- Bédard C, Destexhe A.** Macroscopic models of local field potentials and the apparent 1/f noise in brain activity. *Biophys J* 96: 2589–2603, 2009.
- Bédard C, Kröger H, Destexhe A.** Modeling extracellular field potentials and the frequency-filtering properties of extracellular space. *Biophys J* 86: 1829–1842, 2004.
- Belitski A, Gretton A, Magri C, Murayama Y, Montemurro M, Logothetis NK, Panzeri S.** Low-frequency local field potentials and spikes in primary visual cortex convey independent visual information. *J Neurosci* 28: 5696–5709, 2008.
- Berger H.** Ueber das Elektrenkephalogramm des Menschen. *Arch Psychiat Nervenkr* 87: 527–570, 1929.
- El Boustani S, Marre O, Béhuret S, Baudot P, Yger P, Bal T, Destexhe A, Frégnac Y.** Network-state modulation of power-law frequency-scaling in visual cortical neurons. *PLoS Comput Biol* 5: e1000519, 2009.
- Buzsáki G, Draguhn A.** Neuronal oscillations in cortical networks. *Science* 304: 1926–1929, 2004.
- Buzsaki G.** *Rhythms of the Brain*. New York: Oxford University Press, 2006.
- Chatrian GE.** The mu rhythm. In: *Handbook of Electroencephalography Clinical Neurophysiology: The EEG in the Waking Adult*, edited by Raymond A. Amsterdam, The Netherlands: Elsevier, 1976. p. 46–69.
- Churchland MM, Yu BM, Cunningham JP, Sugrue LP, Cohen MR, Corrado GS, Newsome WT, Clark AM, Hosseini P, Scott BB, Bradley DC, Smith a M, Kohn A, Movshon JA, Armstrong KM, Moore T, Chang SW, Snyder LH, Lisberger SG, Priebe NJ, Finn IM, Ferster D, Ryu SI, Santhanam G, Sahani M, Shenoy KV.** Stimulus onset quenches neural variability: a widespread cortical phenomenon. *Nat Neurosci* 13: 369–78, 2010.
- Crone NE, Boatman D, Gordon B, Hao L.** Induced electrocorticographic gamma activity during auditory perception. *Clin Neurophysiol* 112: 565–582, 2001.
- Crone NE, Miglioretti DL, Gordon B, Lesser RP.** Functional mapping of human sensorimotor cortex with electrocorticographic spectral analysis. II. Event-related synchronization in the gamma band. *Brain* 121: 2301–2315, 1998a.
- Crone NE, Miglioretti DL, Gordon B, Sieracki JM, Wilson MT, Uematsu S, Lesser RP.** Functional mapping of human sensorimotor cortex with electrocorticographic spectral analysis. I. Alpha and beta event-related desynchronization. *Brain* 121: 2271–2299, 1998b.
- Deco G, Jirsa VK, McIntosh AR.** Emerging concepts for the dynamical organization of resting-state activity in the brain. *Nat Rev Neurosci* 12: 43–56, 2011.
- Dehghani N, Bédard C, Cash SS, Halgren E, Destexhe A.** Comparative power spectral analysis of simultaneous electroencephalographic and magnetoencephalographic recordings in humans suggests non-resistive extracellular media. *J Comput Neurosci* 29: 405–421, 2010.
- De la Rocha J, Doiron B, Shea-Brown E, Josić K, Reyes A.** Correlation between neural spike trains increases with firing rate. *Nature* 448: 802–806, 2007.
- Eckhorn R, Bauer R, Jordan W, Brosch M, Kruse W, Munk M, Reitboeck HJ.** Coherent oscillations: A mechanism of feature linking in the visual cortex? *Biol Cybern* 60: 121–130, 1988.
- Fisch L, Privman E, Ramot M, Harel M, Nir Y, Kipervasser S, Andelman F, Neufeld MY, Kramer U, Fried I, Malach R.** Neural “ignition”: enhanced activation linked to perceptual awareness in human ventral stream visual cortex. *Neuron* 64: 562–574, 2009.
- Freeman WJ, Zhai J.** Simulated power spectral density (PSD) of background electrocorticogram (ECoG). *Cogn Neurodyn* 3: 97–103, 2009.
- Fries P, Reynolds JH, Rorie AE, Desimone R.** Modulation of oscillatory neuronal synchronization by selective visual attention. *Science* 291: 1560–1563, 2001.
- Gray CM, Singer W.** Stimulus-specific neuronal oscillations in orientation columns of cat visual cortex. *Proc Natl Acad Sci USA* 86: 1698–1702, 1989.
- Gutnisky DA, Dragoi V.** Adaptive coding of visual information in neural populations. *Nature* 452: 220–224, 2008.
- He BJ, Zempel JM, Snyder AZ, Raichle ME.** The temporal structures and functional significance of scale-free brain activity. *Neuron* 66: 353–369, 2010.
- He BJ.** Scale-free brain activity: past, present, and future. *Trends Cogn Sci* 18: 480–487, 2014.
- Henrie JA, Shapley RM.** LFP power spectra in V1 cortex: the graded effect of stimulus contrast. *J Neurophysiol* 94: 479–490, 2005.
- Janca R, Jezdik P, Cmejla R, Tomasek M, Worrell G, Stead M, Wagenaar J, Jefferys JR, Krsek P, Komarek V, Jiruska P, Marusic P.** Detection of interictal epileptiform discharges using signal envelope distribution modeling: application to epileptic and nonepileptic intracranial recordings. *Brain Topogr* 28: 172–183, 2015.
- Jia X, Xing D, Kohn A.** No consistent relationship between gamma power and peak frequency in macaque primary visual cortex. *J Neurosci* 33: 17–25, 2013.
- Lachaux JP, Rodriguez E, Martinerie J, Adam C, Hasboun D, Varela FJ.** A quantitative study of gamma-band activity in human intracranial recordings triggered by visual stimuli. *Eur J Neurosci* 12: 2608–2622, 2000.
- Logothetis NK, Kayser C, Oeltermann A.** In vivo measurement of cortical impedance spectrum in monkeys: implications for signal propagation. *Neuron* 55: 809–823, 2007.
- Manning JR, Jacobs J, Fried I, Kahana MJ.** Broadband shifts in local field potential power spectra are correlated with single-neuron spiking in humans. *J Neurosci* 29: 13613–13620, 2009.
- Miller KJ, Shenoy P, Nijs Den M, Sorensen LB, Rao RPN, Ojemann JG.** Features in movement classification. *IEEE Trans Biomed Eng* 55: 1634–1637, 2008.
- Miller KJ, Sorensen LB, Ojemann JG, den Nijs M.** Power-law scaling in the brain surface electric potential. *PLoS Comput Biol* 5: e1000609, 2009.
- Milstein J, Mormann F, Fried I, Koch C.** Neuronal shot noise and Brownian 1/f² behavior in the local field potential. *PLoS One* 4: e4338, 2009.
- Minear M, Park D.** A lifespan database of adult facial stimuli. *Behav Res Methods Instruments Comput* 36: 630–633, 2004.
- Mitchell SJ, Silver RA.** Shunting inhibition modulates neuronal gain during synaptic excitation. *Neuron* 38: 433–445, 2003.
- Mukamel R, Fried I.** Human intracranial recordings and cognitive neuroscience. *Annu Rev Psychol* 63: 511–537, 2011.
- Mukamel R, Gelbard H, Arieli A, Hasson U, Fried I, Malach R.** Coupling between neuronal firing, field potentials, and fMRI in human auditory cortex. *Science* 309: 951–954, 2005.
- Nir Y, Fisch L, Mukamel R, Gelbard-Sagiv H, Arieli A, Fried I, Malach R.** Coupling between neuronal firing rate, gamma LFP, and BOLD fMRI is related to interneuronal correlations. *Curr Biol* 17: 1275–1285, 2007.
- Nir Y, Mukamel R, Dinstein I, Privman E, Harel M, Fisch L, Gelbard-Sagiv H, Kipervasser S, Andelman F, Neufeld MY, Kramer U, Arieli A, Fried I, Malach R.** Interhemispheric correlations of slow spontaneous neuronal fluctuations revealed in human sensory cortex. *Nat Neurosci* 11: 1100–1108, 2008.
- Ossandón T, Vidal JR, Ciumas C, Jerbi K, Hamamé CM, Dalal SS, Bertrand O, Minotti L, Kahane P, Lachaux JP.** Efficient “pop-out” visual search elicits sustained broadband γ activity in the dorsal attention network. *J Neurosci* 32: 3414–3421, 2012.
- Ostojic S, Brunel N, Hakim V.** How connectivity, background activity, and synaptic properties shape the cross-correlation between spike trains. *J Neurosci* 29: 10234–10253, 2009.
- Pereda E, Gamundi A, Rial R, González J.** Non-linear behaviour of human EEG: fractal exponent versus correlation dimension in awake and sleep stages. *Neurosci Lett* 250: 91–94, 1998.
- Pfurtscheller G, Aranibar A.** Event-related cortical desynchronization detected by power measurements of scalp EEG. *Electroencephalogr Clin Neurophysiol* 42: 817–826, 1977.
- Pritchard WS.** The brain in fractal time: 1/f-like power spectrum scaling of the human electroencephalogram. *Int J Neurosci* 66: 119–129, 1992.
- Privman E, Nir Y, Kramer U, Kipervasser S, Andelman F, Neufeld MY, Mukamel R, Yeshurun Y, Fried I, Malach R.** Enhanced category tuning

- revealed by intracranial electroencephalograms in high-order human visual areas. *J Neurosci* 27: 6234–6242, 2007.
- Ramot M, Fisch L, Harel M, Kipervasser S, Andelman F, Neufeld MY, Kramer U, Fried I, Malach R.** A widely distributed spectral signature of task-negative electrocorticography responses revealed during a visuo-motor task in the human cortex. *J Neurosci* 32: 10458–10469, 2012.
- Scheffer-Teixeira R, Belchior H, Leão RN, Ribeiro S, Tort ABL.** On high-frequency field oscillations (>100 Hz) and the spectral leakage of spiking activity. *J Neurosci* 33: 1535–1539, 2013.
- Schomburg EW, Anastassiou CA, Buzsáki G, Koch C.** The spiking component of oscillatory extracellular potentials in the rat hippocampus. *J Neurosci* 32: 11798–11811, 2012.
- Smith MA, Kohn A.** Spatial and temporal scales of neuronal correlation in primary visual cortex. *J Neurosci* 28: 12591–12603, 2008.
- Talairach J, Tournoux P.** *Co-Planar Stereotaxic Atlas of the Human Brain*. New York: Thieme Medical Publishers, 1988.
- Tan AYY, Chen Y, Scholl B, Seidemann E, Priebe NJ.** Sensory stimulation shifts visual cortex from synchronous to asynchronous states. *Nature* 509: 226–229, 2014.
- Thomson DJ.** Spectrum estimation and harmonic analysis. *Proc IEEE* 70: 1055–1096, 1982.
- Valencia M, López-Azcárate J, Nicolás MJ, Alegre M, Artieda J.** Dopaminergic modulation of the spectral characteristics in the rat brain oscillatory activity. *Chaos, Solitons Fractals* 45: 619–628, 2012.
- Xing D, Shen Y, Burns S, Yeh CI, Shapley R, Li W.** Stochastic generation of gamma-band activity in primary visual cortex of awake and anesthetized monkeys. *J Neurosci* 32: 13873–13880a, 2012.
- Yamamoto Y, Hughson RL.** Extracting fractal components from time series. *Phys D* 68: 250–264, 1993.

